ELSEVIER

Microporous and Mesoporous Materials 35–36 (2000) 495–509

MICROPOROUS AND MESOPOROUS MATERIALS

www.elsevier.nl/locate/micromeso

Genesis of methane activation sites in Mo-exchanged H–ZSM-5 catalysts

Young-Ho Kim [1], Richard W. Borry III, Enrique Iglesia *

Materials Sciences Division, E.O. Lawrence Berkeley National Laboratory and Department of Chemical Engineering, University of California at Berkeley, Berkeley, CA 94720, USA

Received 19 April 1999; received in revised form 15 June 1999; accepted for publication 22 June 1999

Dedicated to the late Werner O. Haag in appreciation of his outstanding contributions to heterogeneous catalysis and zeolite science

Abstract

Exchanged $(Mo_2O_7)^{2-}$ dimers form during treatment in air of MoO_3/H–ZSM-5 (Si/Al = 14.3) physical mixtures at 773–973 K. The amount of water desorbed during exchange and the number of residual protons (measured by D_2–OH exchange) showed that each Mo^{6+} replaces 1.1 ($\pm$0.1) protons in H–ZSM-5 (for Mo/Al < 0.37). ^{27}Al NMR, X-ray absorption, and Raman spectra confirmed the proposed $(Mo_2O_7)^{2-}$ structure and its location at zeolite exchange sites. When the Mo content exceeds that required to form a MoO_x bilayer on the external zeolite surface (Mo/Al $\approx$ 0.5), MoO_x sublimes or forms $Al_2(MoO_4)_3$ by extracting framework Al; $Al_2(MoO_4)_3$ domains reduce slowly and lead to low CH_4 reaction rates. The rate of hydrocarbon synthesis from CH_4 at 930–973 K increased as exchanged MoO_x dimers reduce and carburize during CH_4 reactions. About 2.5 O atoms per Mo ($\pm$0.1) are removed as CO, CO_2, and H_2O during activation, suggesting that all but the zeolite framework oxygen atoms are removed during activation. Reduction and carburization rates depend on Mo content and on the rate of removal of CO, CO_2, and H_2O, which inhibit reduction/carburization steps.

Hydrocarbons were not detected during the initial removal of about one O per Mo, but ethylene, benzene, naphthalene, and H_2 formation rates increased as larger amounts of O were removed during CH_4 reactions. CH_4 reactions require initial activation of CH_4 on MoO_x, but with the retention of C-atoms to form MoC_x. These MoC_x then activate C—H bonds and desorb the hydrocarbons formed, which then oligomerize and cyclize via rapid bifunctional pathways on H^+ and MoC_x sites within constrained ZSM-5 channels.

Keywords: Methane; Mo carburization; Mo/H–ZSM-5; Mo structure; Pyrolysis

* Corresponding author. Tel.: +1-510-642-9673; fax: +1-510-642-4778.

E-mail address: iglesia@cchem.berkeley.edu (E. Iglesia)

[1] Permanent address: Kunsan National University, Kunsan, Chonbuk 573-701, South Korea.

1387-1811/00/$ - see front matter
PII: S1387-1811(99)00245-0

1. Introduction

Cation-exchanged H–ZSM-5 materials are widely used as catalysts for the activation of light alkanes [1–3]. Steric constraints imposed by zeolite channels limit chain growth and prevent the formation of large aromatics, which can lead to deactivation and to loss of selectivity during alkane conversion reactions. Recently, Mo/H–ZSM-5 has been reported to convert CH_4 to equilibrium benzene yields at 973 K, without significant yields of products larger than naphthalene [4–6].

Mo/H–ZSM-5 catalysts have been prepared by slurry or incipient wetness impregnation of H–ZSM-5 with aqueous ammonium heptamolybdate [AHM; $(NH_4)_6Mo_7O_{24}$], followed by treatment in air at high temperatures (723–973 K) [4–7]. Large hydrated molybdate ions, however, do not exchange directly onto H–ZSM-5 during aqueous exchange or impregnation [8]. Infrared spectroscopy and differential thermal analysis [9] suggested that AHM decomposes in air between 500 and 650 K to form MoO_3 crystallites on external zeolite surfaces [10,11]. At about 773 K, MoO_3 infrared bands disappear as MoO_3 crystallites disperse on external ZSM-5 surfaces, and ultimately migrate and exchange within zeolite channels [9]. As isolated MoO_x species migrate into ZSM-5 channels via vapor or surface diffusion, they anchor at cation exchange sites by replacing protons in H–ZSM-5. Dealumination and loss of ZSM-5 crystallinity occur concurrently with this exchange process and they lead to the loss of acidic protons.

MoO_x species within zeolite channels are precursors to the active sites required for non-oxidative CH_4 aromatization. MoO_x/H–ZSM-5 catalysts show very low initial CH_4 aromatization rates at 973 K, but the reduction and carburization of highly dispersed MoO_x species into molybdenum carbide lead to the initial conversion of CH_4 to CO_x, H_2, and H_2O, and to significantly higher CH_4 aromatization rates after 0.2–1.0 h on stream [5,6]. MoC_x sites convert CH_4 into ethane and ethylene, which then react to form C_6–C_{10} aromatics on acid sites via rapid oligomerization, cracking, and cyclization reactions. These reactions also benefit from the hydrogen removal function provided by MoC_x sites via pathways similar to those reported on Ga- and Zn-exchanged H–ZSM-5 [12]. Previous CH_4 activation studies on MoO_x/H–ZSM-5 used chromatographic methods in order to measure the initial rate increase and the concurrent reduction and carburization after initial contact of MoO_x/H–ZSM-5 precursors with CH_4. The time resolution of such methods was, however, very low (0.5 h) because of the time required for chromatographic analyses [5,6,13]. These studies showed that H_2O, CO_2, and CO are the predominant gas-phase products until reduction–carburization processes are complete; thereafter, benzene, naphthalene, and ethylene become the most abundant products during steady-state catalysis. The lack of detailed measurements of the extent and rate of reduction and carburization during this initial carburization process has led to conflicting proposals about the structure and the stoichiometry of the Mo active sites required for C—H bond activation. X-ray photoelectron spectroscopy suggested that Mo_2C species exist in activated catalysts [6]. MoO_xC_y species were proposed based on CH_4 reaction rates on partially oxidized Mo_2C/H–ZSM-5 catalysts [14].

In this study, MoO_x/H–ZSM-5 was prepared by solid-state exchange methods using physical mixtures of MoO_3 and H–ZSM-5. This synthesis method eliminates the evolution of large amounts of N_2, NH_3, and H_2O during subsequent air treatment [9] and it allows accurate measurements of the nature and rate of MoO_x exchange from the water evolved from condensation reactions of OH groups. Our study addresses the synthesis of MoO_x/H–ZSM-5 from mixtures of MoO_3 and H–ZSM-5, and the structure and density of Mo and acid sites in both catalyst precursors and active catalysts. We also report here detailed measurements of the rate of oxygen removal and of the rate and selectivity of CH_4 conversion during the activation of MoO_x/H–ZSM-5 precursors with a wide range of Mo content (Mo/Al = 0–0.68).

2. Experimental

NH_4–ZSM-5 was prepared by sequential aqueous exchange of Na/ZSM-5 (Zeochem, Si:Al =

14.3) with fresh 1.0 M NH_4NO_3 (Fisher) solutions (~10 g ZSM-5 per liter; repeated four times). The samples were then dried at 400 K for 24 h and treated in dry air at 773 K for 24 h (~10 g ZSM-5, 100 cm^3/min air) to yield H–ZSM-5. Mo/H–ZSM-5 samples were prepared from physical mixtures of MoO_3 (Johnson Matthey, 99.5% purity) and H–ZSM-5 initially containing 1, 2, 4, and 8 wt% Mo. These mixtures were prepared by initially grinding the two solids for about 0.2 h using an alumina mortar and pestle. Powder X-ray diffraction patterns were obtained with a Siemens Diffractometer D5000 using Cu Kα radiation (λ = 1.5406 Å). Micropore volumes were obtained from N_2 physisorption at 77 K using an Autosorb 6 automated surface area analyzer (Quantachrome, Inc.).

The effect of thermal treatment in air on the structure and catalytic properties of MoO_x/H–ZSM-5 samples was examined using MoO_3/H–ZSM-5 mixtures (0.3 g, 0–8 wt% Mo; Mo/Al = 0–0.87) dried at 623 K for 24 h in 20% O_2/Ar (100 cm^3/min). Samples were heated at 0.16 K s^{-1} to 973 K and H_2O evolution rates were measured by mass spectrometry (Leybold Inficon, THP-TS200) with a time resolution of 2 s using heated transfer lines (373 K) and Ar as an internal standard. Samples were held at 973 K for 0.5 h and then cooled to 300 K. The Mo content of samples after oxidation at 973 K was determined using atomic absorption spectroscopy. The ^{27}Al NMR procedure was reported in detail previously [13]. Tetrahedral Al in the ZSM-5 framework has a chemical shift of 56 ppm [relative to dilute $Al(NO_3)_3$ solutions]; octahedral extra-framework Al species in ZSM-5 and Al_2O_3 show no chemical shift and $Al_2(MoO_4)_3$ (octahedral Al, tetrahedral Mo centers) shows an NMR line at −13 ppm [15].

The number of H atoms remaining as OH groups in air-treated MoO_x/H–ZSM-5 samples was measured by heating these samples from 300 K to 873 K (0.16 K s^{-1}, 120 s hold time) in flowing 5% D_2–Ar (100 cm^3/min) while monitoring the evolution of HD and H_2 by mass spectrometry [12]. The rate of carburization of MoO_x/H–ZSM-5 samples was measured at 950 K after treating exchanged MoO_x/H–ZSM-5 samples at 950 K in 20% O_2–He (100 cm^3/min, Matheson, >99.999% purity) for 0.5 h. The samples were flushed with He (100 cm^3/min), then exposed to reactants (CH_4:Ar = 1:1, 100 cm^3/min, Praxair Inc. 99.95% purity). Argon was used as an internal standard in order to calculate the rates of CH_4 conversion and of CO_x, H_2, H_2O, and hydrocarbon formation, and the amount of carbon left on the catalyst and in the transfer lines. The effluent was sampled into a mass spectrometer (Leybold-Inficon) through a differentially pumped chamber and a capillary leak tube in order to avoid mass discrimination. Accurate measurements of multiple species with overlapping mass fragmentation patterns required deconvolution of the mass spectra using fragmentation patterns and calibrated response factors for each product, as described in detail elsewhere [16].

3. Results and discussion

3.1. Structure and density of MoO_x species formed from MoO_3/H–ZSM-5 physical mixtures

CH_4 reaction rates on Mo/H–ZSM-5 samples prepared by solid-state reactions of MoO_3/H–ZSM-5 physical mixtures [13] and on samples prepared by impregnation of H–ZSM-5 with aqueous AHM [6] were very similar [13]. During treatment in air at high temperatures (~973 K), MoO_x species in both samples spread on external zeolite surfaces and then migrated into zeolite channels and replaced H^+ present at cation exchange sites [13].

H_2O evolution was detected between 673 and 973 K during temperature-programmed oxidation (TPO) of MoO_3/H–ZSM-5 mixtures, even after physisorbed water was completely removed by drying samples at 623 K for 24 h (Fig. 1). Below 740 K, the rate and amount of H_2O evolved did not depend on Mo content (Fig. 2), suggesting that it arises from the condensation of neighboring OH groups with the displacement of Al cations from their crystallographic positions in the ZSM-5 framework [17]. Between 740 and 840 K, H_2O desorption rates increase with increasing Mo content (Fig. 2). This desorption feature reflects

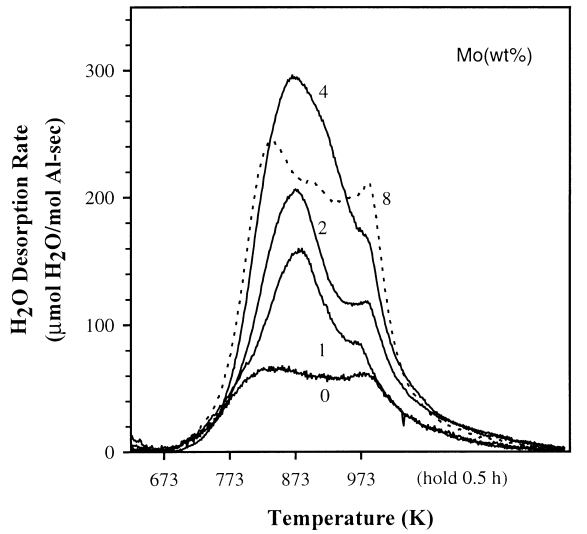

Fig. 1. H_2O desorption between 623 and 973 K from MoO_3/H–ZSM-5 mixtures with varying Mo initial concentration (0.3 g, 100 cm^3/min, 20% O_2–Ar, heat at 0.16 K s^{-1}, hold at 973 K for 0.5 h).

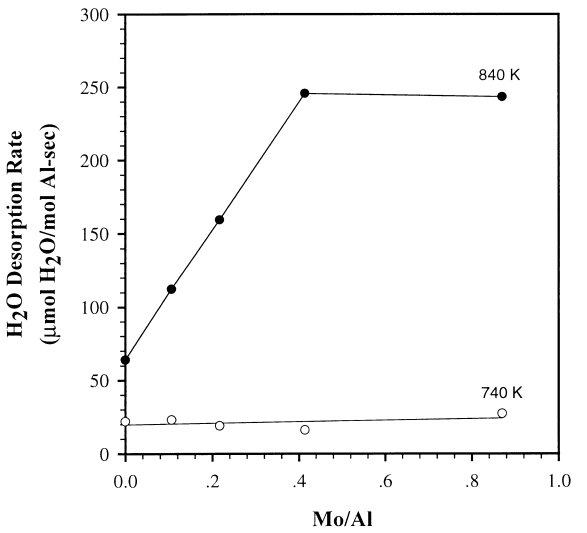

Fig. 2. H_2O desorptioin rate during TPO of MoO_3/H–ZSM-5 mixtures at 740 and 840 K (from Fig. 1) Mo/Al ratios are as prepared. Mo concentrations after TPO are shown in Table 1.

the replacement of H^+ species by Mo-oxo cations and the anchoring of MoO_x species via condensation reactions [13].

Elemental analysis of samples after treatment in air showed that samples containing more than 2 wt% Mo lost some MoO_x due to sublimation (Table 1). In the rest of this paper, initial Mo concentrations will be used when discussing treatments of the starting physical mixtures; Mo concentrations in the final MoO_x/H–ZSM-5 samples will be used in describing all characterization and catalytic studies after synthesis. Initial and final Mo contents for each sample are shown in Table 1.

The initial H_2O desorption rates (between 740 and 840 K) were very similar on MoO_3/H–ZSM-5 mixtures containing 4 and 8 wt% Mo (Figs. 1 and 2). At higher temperatures, however, the curve for the 8 wt% Mo sample differs from those for samples with 1–4 wt% Mo (Fig. 1). Elemental analysis after treatment in air at 973 K for 0.5 h showed that about 19.3% of the Mo in the mixture sublimed and formed small MoO_3 crystallites on the reactor walls just outside the heated zone (Table 1). X-ray diffraction and N_2 physisorption results showed significant loss of zeolite crystallinity and micropore volume on the sample with the highest Mo content [13]. ^{27}Al NMR spectroscopy showed that this sample contained only $Al_2(MoO_4)_3$ domains after treatment. Samples with less Mo (1–4 wt%), however, did not show any NMR lines characteristic of $Al_2(MoO_4)_3$ [13]. The unusual H_2O evolution profile for the sample with the highest Mo content (Fig. 1) reflects the extraction of Al from crystallographic framework positions in ZSM-5 to form stable $Al_2(MoO_4)_3$ domains with the concomitant collapse of zeolite channels. These structural changes occur above 840 K and they lead to the unusual H_2O evolution curves on mixtures with high Mo content (Figs. 1 and 2). The formation of $Al_2(MoO_4)_3$ domains and the loss of zeolite crystallinity was previously reported on MoO_x/H–ZSM-5 samples with 3–15 wt% Mo prepared by aqueous methods and treated in air at 773–973 K [15]. Mixtures with Mo contents below about 5 wt% form MoO_x monolayers on external zeolite surfaces ($\sim 25\ m^2\ g^{-1}$), which gradually migrate within zeolite channels to form anchored $(MoO_x)_n$ species [13]. Excess MoO_3 remains as

Table 1
Mo content of MoO_3/H–ZSM-5 mixtures before and after air treatment to 973 K (0.5 h), and micropore volume (from N_2 physisorption at 77 K) of treated samples

Mo in mixture (wt%)	Mo/Al ratio[a]	Mo content after preparation (wt%)	Mo/Al ratio after preparation	Micropore volume (cm^3/g ZSM-5)
0	0	0	0	0.128
1	0.11	1.07	0.11	0.119
2	0.21	2.00	0.20	0.120
4	0.42	3.60	0.37	0.107
8	0.87	6.34	0.68	0.059

[a] Mo/Al ratio calculated from wt% Mo and Si/Al ratio (14.3) of H-ZSM-5.

small crystallites, which sublime as MoO_3 oligomers or melt. Either process leads to their migration within zeolite channels where they provide nucleation sites for the formation of thermodynamically stable, but catalytically inactive, $Al_2(MoO_4)_3$ domains.

The intensity of ^{27}Al NMR lines corresponding to Al centers at tetrahedral framework positions and containing O—H groups ($\delta = 56$ ppm) decreased as the Mo content increased, even for samples with low Mo content (1–4 wt%; Fig. 3). Water evolution from pure H–ZSM-5 at 673–973 K reflects the condensation of next-nearest neighbor hydroxyl groups at Al sites to form Al—O—Al species that cannot remain in the tetrahedral symmetry required by the zeolite framework. The loss of Brønsted acid sites occurs concurrently with the local disruption of the zeolite structure, which distorts Al centers from their pure tetrahedral symmetry and causes, at even higher temperatures, the nucleation of Al_2O_3 domains with octahedral Al centers. These hydroxyl condensation events also occur in MoO_3/H–ZSM-5 mixtures during treatment in air. Therefore, we have estimated the framework Al centers (Al_F) remaining in MoO_3/H–ZSM-5 samples by subtracting the number of Al atoms extracted from the framework (from the H_2O evolved from H–ZSM-5) from the total number of Al atoms in the sample (Si/Al = 14.3). This corrected Al_F content is used in reporting hydroxyl densities as H/Al_F (Table 2).

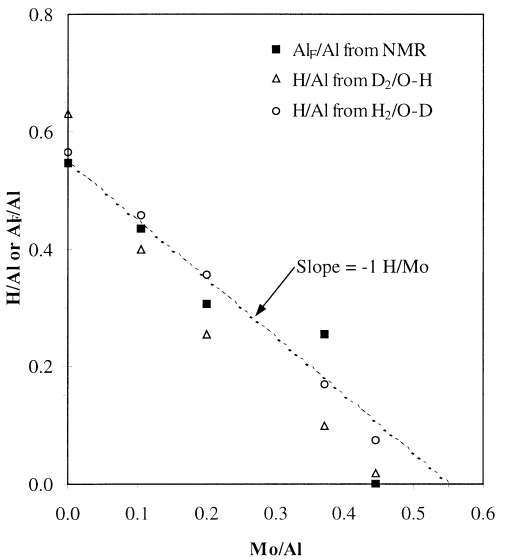

Fig. 3. Number of acids sites (H) or framework Al (Al_F) remaining per total Al for series of Mo/H–ZSM-5 samples after TPO and TPR treatment to 973 K (0.5 h) measured by ^{27}Al NMR, D_2/O—H, and H_2/O—D. Reported Mo/Al ratios are after air treatment to 973 K, 0.5 h.

The exchange of D_2(g) with O—H groups has been used to measure the density of the remaining OH groups in H–ZSM-5 after aqueous exchange of H^+ by Zn^{2+} cations [12].

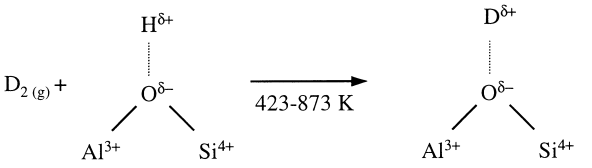

Table 2
H_2O desorption (TPO, 0.3 g, 100 cm^3/min, 20% O_2 in He) and isotopic exchange (0.16 K s^{-1}, 100 cm^3/min, 5% D_2 in Ar) of MoO_3/H–ZSM-5 mixtures

Mo content after TPO (wt%)	Mo/Al ratio	H_2O desorption			Residual H content
		H/Al[a]	H/Al^b_F	H/Mo[c]	H/Al[d]
0	0	0.229	0	–	0.630
1.0	0.11	0.347	0.118	1.11	0.400
2.0	0.20	0.474	0.245	1.22	0.254
3.6	0.37	0.686	0.457	1.23	0.099
6.3	0.68	0.665	0.436	0.64	0.035

[a] From integrated area of H_2O desorption above 623 K (Fig. 1).
[b] Subtract value in column to the left from that for H–ZSM-5 (0 wt% Mo).
[c] Divide value in column to the left by Mo/Al ratio.
[d] From D_2(g)/O(s)—H isotopic exchange (Fig. 4).

In MoO_3/H–ZSM-5 mixtures, the number of residual OH groups after treatment in air at 973 K for 0.5 h was obtained from the amount of HD and H_2 evolved during exchange of D_2 with OH groups (Figs. 3 and 4; Table 2). The density of OH groups decreased linearly with increasing Mo content, suggesting that each MoO_x species replaces a single H^+ in physical mixtures with 1–4 wt% Mo. These data also suggest that the nature of exchanged Mo species is similar in all samples with 1–4 wt% Mo (Mo/Al = 0–0.42). Fig. 5 shows the number of OH/Al replaced by MoO_x during exchange (from H_2O desorption) and the number of remaining OH/Al remaining after exchange (from D_2 exchange) as a function of the Mo/Al ratio in the samples. The sum of the remaining OH groups and those removed is very similar in all samples and about equal to the number of OH groups remaining after treatment in air on pure H–ZSM-5. The materials prepared by exchange from physical mixtures of MoO_3 and H–ZSM-5 show a single type of MoO_x species, something that is rarely achieved in the synthesis of heterogeneous catalysts.

The amount of water evolved between 673 and 973 K during treatment of MoO_3/H–ZSM-5 mixtures in air shows that each MoO_x replaces O—H groups with a stoichiometry of 1 ± 0.2 H/Mo for mixtures containing 1–4 wt% Mo (Table 2;

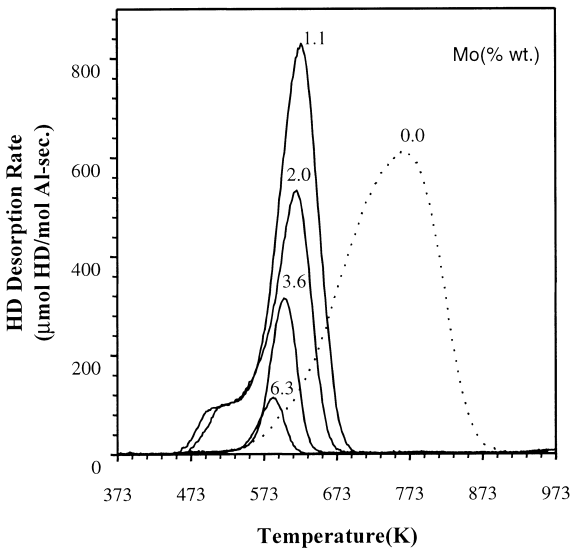

Fig. 4. Rate of HD desorption during D_2(g)/O—H(s) isotopic exchange on Mo/H–ZSM-5 (0.3 g, 100 cm^3/min 5% D_2–Ar, 101 kPa). Mo concentrations shown are after air treatment to 973 K, 0.5 h.

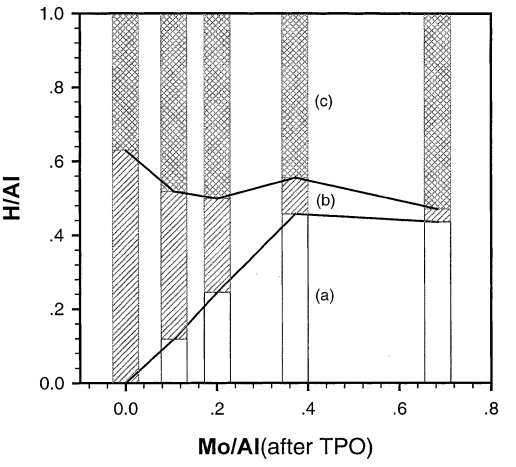

Fig. 5. Number of acid sites (H^+) per total Al for series of Mo/H–ZSM-5 samples from H_2O desorption during TPO. (b) from D_2/O—H (the remaining Brønsted acid) and (c) the balance (from condensation of acid sites and structural rearrangement). Reported Mo/Al ratios are after air treatment to 973 K, 0.5 h.

Figs. 3 and 5).

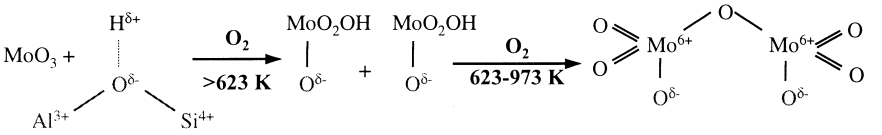

These data, the requirement for charge balance, ^{27}Al NMR [13] and X-ray absorption [18] results previously reported show that MoO_x species exist at exchange sites as isolated $(Mo_2O_7)^{2-}$ ditetrahedra containing framework oxygen atoms associated with two Al sites. In contrast, samples prepared from mixtures initially containing 8 wt% Mo (6.24 wt% after exchange) give a replacement stoichiometry of H/Mo ratio of 0.64, in agreement with the value expected for the formation of $Al_2(MoO_4)_3$ domains (H/Mo = 0.67).

3.2. Activation of MoO_x/H–ZSM-5 precursors during CH_4 reactions

$(Mo_2O_7)^{2-}$ dimers formed during synthesis do not catalyze CH_4 conversion to hydrocarbons, but they form active Mo—C centers by using CH_4 to reduce and carburize MoO_x species at 950–1000 K [13], as also reported by others [6,14]. Mass spectrometric analysis with matrix deconvolution of complex overlapping spectra was used in order to measure the evolution of reaction products and the kinetics of reduction and carburization of MoO_x precursors during the initial contact with CH_4. The time resolution of the data was about 2 s. A deconvolution matrix was developed from the mass spectra of each product detected by gas chromatography. Response factors were obtained by matching the product yields obtained by mass spectrometry with quantitative analyses by gas chromatography using flame ionization and thermal conductivity detection [16].

Reactant (CH_4) and product (H_2O, H_2, CO, CO_2, C_2H_4, C_2H_6, C_3H_6, C_3H_8, benzene, toluene, naphthalene) concentrations were measured on MoO_x/H–ZSM-5 (0.5 g) prepared from mixtures with 1–8 wt% Mo using a 50% CH_4–Ar mixture (100 cm^3/min) at 950 K. Typical results are shown in Fig. 6 for one of the MoO_x/H–ZSM-5 samples (3.6 wt% Mo); the trends on the other samples were similar. In all MoO_x/H–ZSM-5 samples, CO_2 and H_2O formed as the predominant initial products. These products form via reactions of CH_4 with O-atoms in MoO_x precursors. As O-atoms in MoO_x are depleted by reduction, CO and H_2 become the predominant gas-phase products. Hydrocarbons ultimately become the catalytic products of CH_4 reactions as oxygen removal rates decrease; C_2, C_3, and aromatics (benzene, toluene and naphthalene) were detected in the gas phase as CO and H_2 formation rates decreased. As isolated molybdenum carbide species are formed, catalytic CH_4 conversion begins, producing C_2H_4 products. C_2H_4 is then rapidly converted to aromatics on acid sites in H–ZSM-5.

The total amount of oxygen removed as CO, CO_2, and H_2O reflects the extent of reduction of $(Mo_2O_7)^{2-}$ dimers. The oxygen removal rate and the cumulative amount of oxygen removed during CH_4 reactions at 973 K are shown in Fig. 7 for MoO_x/H–ZSM-5 samples containing 1.1, 2.0, 3.6, and 6.34 wt% Mo. Oxygen removal rates (per Mo atom) are initially similar in all samples, but the later stages of reduction become slower as the Mo content increases. This reflects the inhibition effect of reduction products on the rate of reduction and carburization, an effect that becomes stronger as the concentrations of these products increase with increasing amount of MoO_x (at a constant CH_4 flow rate). As a result, the time required to complete reduction–carburization processes and to reach steady-state rates of CH_4 conversion to higher hydrocarbons increases with increasing Mo content. These effects are described in greater detail below. The total number of oxygen atoms removed during activation (O_{rem}/Mo) approaches a value of 2.5 ($\pm$0.2) for samples with 1.0–3.6 wt% Mo, consistent with the removal of all oxygen atoms from $(Mo_2O_7)^{2-}$, except those in the zeolite framework, during the induction period.

Oxygen removal rates are much lower on the

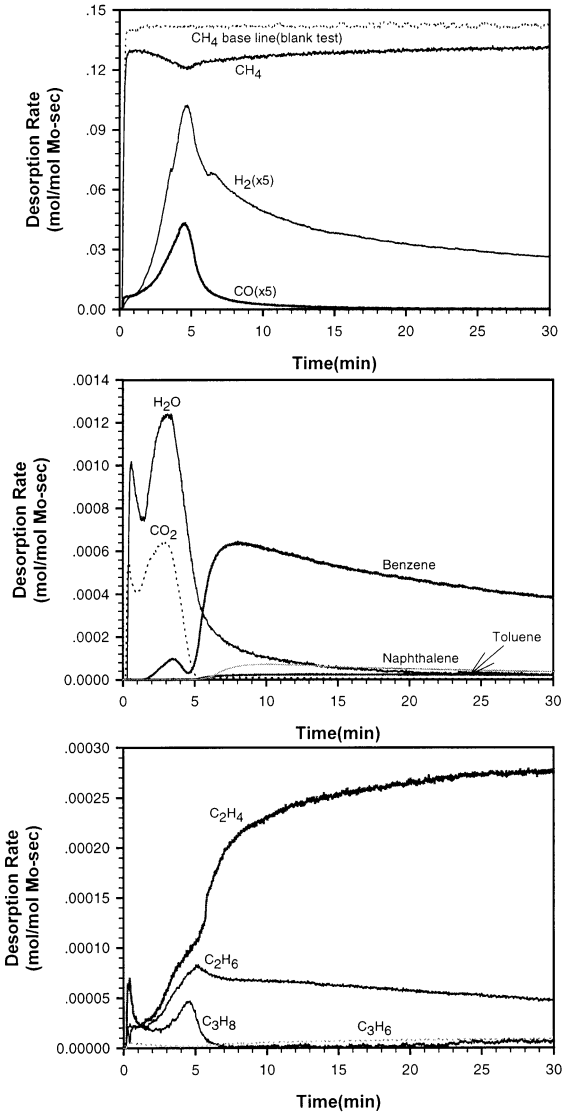

Fig. 6. Desorption rates of products during start-up period of CH_4 activations (0.5 g, 3.6 wt% Mo/H–ZSM-5, 950 K, 100 cm^3/min 1:1 CH_4/Ar).

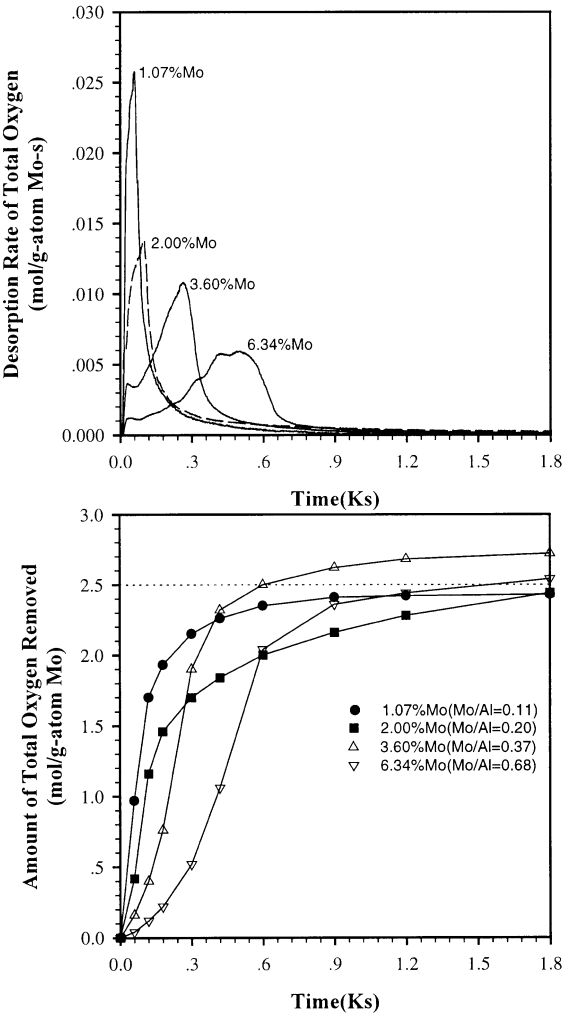

Fig. 7. Total desorption rates of all oxygen-containing compounds (top, mol O/g-atom Mo-s) and the cumulative oxygen removed (O_{rem}/Mo, bottom) versus time during the start-up period of CH_4 activation (0.5 g, 950 K, 100 cm^3/min 1:1 CH_4/Ar).

sample with the highest Mo content (6.3 wt%), which contains predominantly $Al_2(MoO_4)_3$ domains. Yet, the amount of oxygen removed (O/Mo $\approx$ 2.5) is similar to that on samples containing exchanged Mo dimers, instead of that expected from the complete reduction of Mo^{6+} to Mo^0 in $Al_2(MoO_4)_3$ domains. These results suggest that such domains retain some Mo—O—Al bonds during reduction and carburization in CH_4 at 973 K. Bulk $Al_2(MoO_4)_3$ is difficult to reduce in H_2 or CH_4 atmospheres below 1000–1200 K [19]. Dispersed $Al_2(MoO_4)_3$ species in H–ZSM-5, however, reduce and carburize during the initial stages of CH_4 conversion reactions, albeit much more slowly than $(Mo_2O_7)^{2-}$ species. Bulk $Al_2(MoO_4)_3$ appears to lack the C—H bond activation sites required to initiate reduction/carburization reactions in CH_4 atmospheres. This suggests that coor-

Table 3
CH_4 conversion and carbon selectivity in gas-phase products during initial activation period on Mo/H–ZSM-5 catalysts (values reported are those at the point of maximum hydrocarbon yield)

Catalyst (wt% Mo)	1.1	2.0	3.6	6.3
CH_4 conversion rate (10^{-2} CH_4/Mo-s)	6.12	3.66	1.60	0.22
CH_4 conversion (%)	10.7	13.2	11.1	3.4
Selectivity (%)				
C_2H_4	8.2	7.6	8.2	10.2
C_6–C_{10} aromatics	87.6	88.8	88.9	84.7
C_2H_4/aromatics ratio	0.09	0.09	0.09	0.12

dinatively unsaturated surface sites, co-existing minority $(Mo_2O_7)^{2-}$ species, or even sites in ZSM-5 (e.g. defects, extra-framework Al, or metal impurities) may provide the C—H activation sites required to initiate the reduction and carburization of the dispersed $Al_2(MoO_4)_3$ species present in the 6.3 wt% Mo/H–ZSM-5 sample.

Table 3 shows CH_4 conversion rates and product selectivities on all Mo/H–ZSM-5 samples used in this study. The similar CH_4 conversions obtained on MoO_x/H–ZSM-5 samples with 1.1–3.6 wt% Mo reflect the near-equilibrium conditions achieved at the reactor exit on all samples. As a result, apparent CH_4 conversion rates (per Mo) decrease with increasing Mo content. The lower CH_4 conversions reached on the sample with the highest Mo content (6.3 wt%) appear to reflect the formation of poorly dispersed MoC_x species during reduction and carburization of $Al_2(MoO_4)_3$ domains and the loss of acid sites due to structural degradation of ZSM-5.

Earlier studies [6,20] have shown that CH_4 conversion on Mo/H–ZSM-5 occurs via a sequential pathway involving CH_4 activation on MoC_x sites to form C_2H_4, followed by acid-catalyzed chain growth reactions of C_2H_4 aided by dehydrogenation and hydrogen removal steps on MoC_x sites and occurring within shape-selective ZSM-5 channels. The accompanying steric constraints limit chain growth to naphthalene and larger molecules.

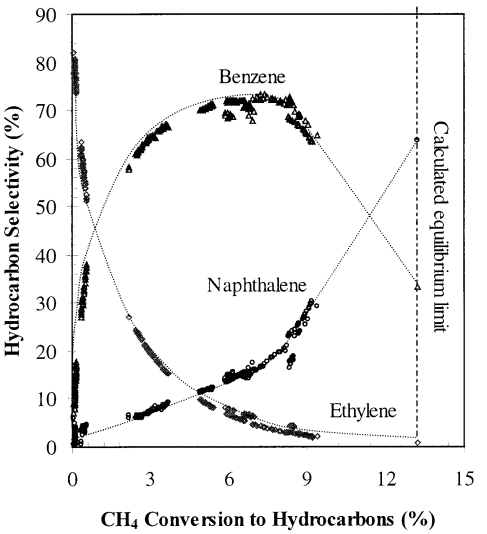

Fig. 8. CH_4 conversion into C_2–C_{10} hydrocarbons versus product selectivity, excluding CO_x and solid carbon (950 K, 0.5–1.0 g 4% Mo/H–ZSM-5, 5–50 cm^3/min 1:1 CH_4/Ar, 0–96 h reaction time).

Fig. 8 shows product selectivities on 4 wt% Mo/H–ZSM-5 at 950 K as a function of conversion. CH_4 conversion was varied by changing the reactor residence time and by allowing the catalyst to deactivate during CH_4 reactions. These selectivity–conversion curves demonstrate that CH_4 reacts sequentially to form C_2H_4 as initial reactive products, C_6H_6 as a secondary product, and naphthalene as the kinetic end point (except for its slow conversion to condensed multi-ring aromatics). The rapid removal of C_2H_4 (via aromatization) removes thermodynamic and kinetic constraints that would otherwise limit CH_4 conversion to C_2H_4 to about 3.8% at 950 K. The similar trends observed when conversion is varied by varying residence time or the number of active sites (via deactivation) show that deactivation removes active sites from the catalyst without any changes in the catalytic properties of the remaining active sites.

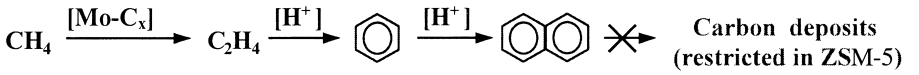

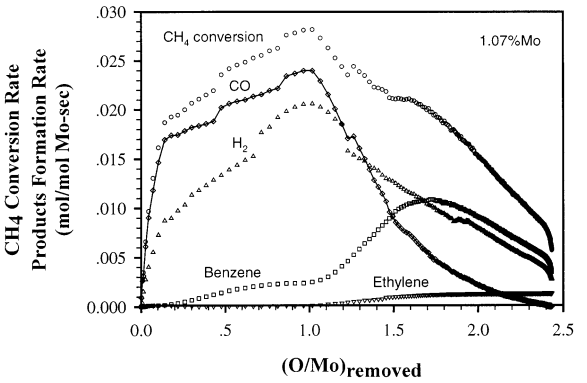

Fig. 9. CH_4 conversion and product (H_2, CO, C_6H_6, C_6H_6, C_2H_4) formation rates as a function of the amount of oxygen removed during initial reduction–carburization period on 1.07 wt% Mo/H–ZSM-5 (reaction conditions same as in Figs. 6 and 7).

3.3. Evolution of CH_4 conversion rates during reduction and carburization

The effect of the amount of oxygen removed on CH_4 conversion and product formation rates is shown in Fig. 9 for the 1 wt% MoO_x/H–ZSM-5 sample and in Figs. 10 and 11 for all MoO_x/H–ZSM-5 catalysts. The rate of methane conversion increases markedly with the initial removal of oxygen from the catalyst, but the predominant products are H_2 (Fig. 9), CO (Fig. 9), CO_2, and H_2O. After removal of about one O atom per Mo, the rate of reduction/carburization decreases and the rate of formation of hydrocarbons begins to increase until it reaches maximum ethylene and benzene formation rates as the amount of oxygen removed (O/Mo) reaches 1.5–1.9. This behavior suggests that the reduction proceeds in two steps. The first step involves the reduction of Mo^{6+} to Mo^{4+} with the formation of sites that activate methane but which do not desorb hydrocarbon fragments, but instead retain C atoms from CH_4 and release H atoms as H_2. The second reduction step is slower and it leads directly to the formation of sites active for methane conversion, but these sites form sequentially along the catalyst bed, because of the inhibition of reduction/carburization processes by the oxygen-containing products of this reaction. Maximum rates of formation of benzene and ethylene are

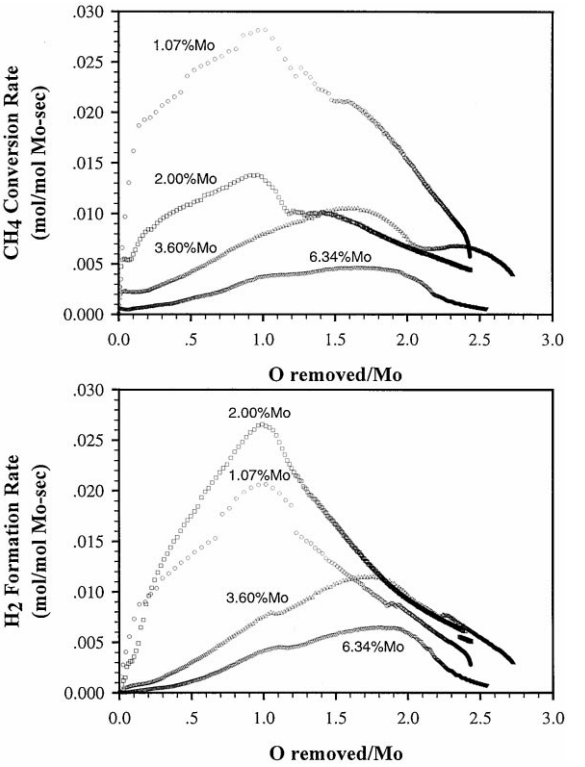

Fig. 10. CH_4 conversion rate to hydrocarbons (top) and H_2 formation rate (bottom) as a function of the amount of oxygen removed (O/Mo) during initial reduction–carburization (conditions: the same as in Figs. 6 and 7).

achieved before complete reduction/carburization takes place because deactivation has decreased the conversion rates by the time the entire bed has been carburized and the last remaining oxygen atoms have been removed. An alternate explanation is that sites that activate C—H bonds and allow the removal of adsorbed hydrocarbons before complete dehydrogenation to carbon require the presence of some residual O-atoms in MoC_x species. Such species, however, appear to reduce further and they cannot be maintained during CH_4 conversion reactions.

The removal of only 2.5 O/Mo suggests that either Mo^+ [specifically $(MoC_NH_X)^+$] species remain anchored at one Al site or that Mo^0 species are removed from Al sites and replaced by H^+ species during reduction. Mo—O bonds have been detected in radial distribution functions derived

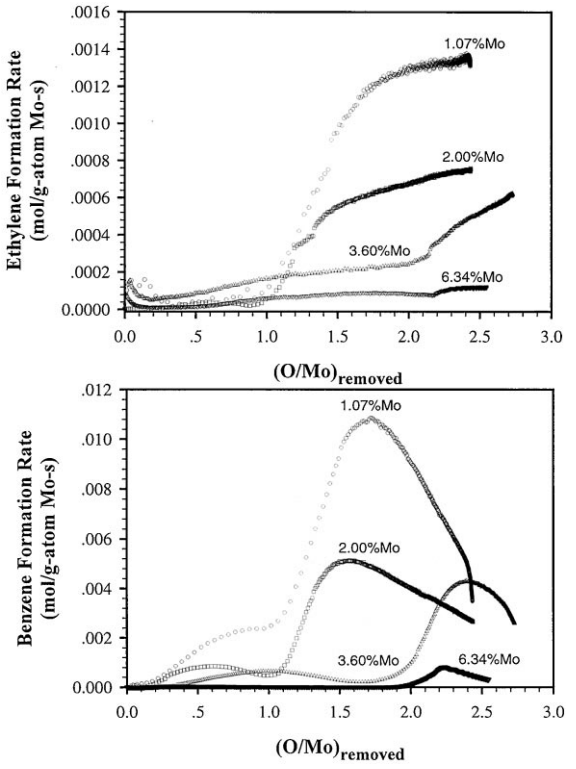

Fig. 11. C_2H_4 formation rate (top) and benzene formation rate (bottom) as a function of the amount of oxygen removed (O/Mo) during initial reduction–carburization (conditions: the same as in Figs. 6 and 7).

from X-ray absorption data [18,21], suggesting that Mo remains attached to framework oxygen atoms and that it retains a non-zero oxidation state. The re-formation of H^+ species during reduction is unlikely because ^{27}Al NMR shows that anchored Mo species significantly distort Al centers from the tetrahedral coordination required to re-form acid centers in ZSM-5. Also, high levels of exchange lead to very low CH_4 conversion rates, suggesting that acid sites removed during exchange do not re-form during carburization or CH_4 conversion reactions.

Figs. 10 and 11 show the rate of CH_4 conversion and formation of H_2, ethylene and benzene on all MoO_x/H–ZSM-5 catalysts as oxygen is removed during reduction–carburization at 973 K. The observed trends are similar on all catalysts. The rates of CH_4 conversion and of H_2 formation increase initially without a concomitant increase in the rate of formation of hydrocarbon products (Fig. 10). CO_x and H_2O also form initially as MoO_x/H–ZSM-5 samples reduce and carburize during contact with CH_4 at 973 K. Samples with 1.1 and 2.0 wt% Mo start to form hydrocarbons after the removal of about one oxygen atom per Mo (Fig. 11). Samples with higher Mo content appear to require a greater extent of reduction before hydrocarbons can be formed at significant rates. Maximum rates are obtained at intermediate times on stream for all samples because side reactions leading to carbon formation deactivate MoC_x sites formed during the initial induction period. Deactivation influences the rate of benzene formation more strongly than the rate of ethylene formation because of the sequential nature of the reaction pathways illustrated by the data in Fig. 8. In effect, deactivation decreases CH_4 conversion levels and the effective reactive residence time of molecules within the catalyst bed. As a result, it moves the product distribution towards the initial products of the reaction sequence.

The effect of space velocity (defined as moles CH_4 fed per g-atom Mo-s) is shown in Fig. 12 for the 3.6 wt% Mo/H–ZSM-5 sample. As the space velocity increases from $0.16\ s^{-1}$ to $0.65\ s^{-1}$, the initial reduction/carburization rate increases (Fig. 12) and it approaches the rates measured on a sample with lower Mo content at the higher value of the space velocity (1.07 wt% Mo; $0.61\ s^{-1}$). These data are consistent with the explanation that reduction rates are inhibited by the products of reduction/carburization steps, as discussed previously. Interestingly, the sample with 3.6 wt% Mo activates more slowly than that with 1.07 wt% Mo, even when the space velocity is maintained at similar values (0.65 versus $0.61\ s^{-1}$). This reflects diffusional restrictions within zeolite crystallites ($\sim$1–2 μm diameter), which cause gradients in the concentration of H_2O and CO_x within crystals as MoO_x precursors reduce and carburize. The higher MoO_x content in the 3.6 wt% sample leads to more severe intraparticle gradients and to a stronger inhibitory effect of products, even when reactor residence times are similar. A qualitative assessment of the severity of intraparticle gradients using the Weisz–Prater criterion [22] supports this conclusion.

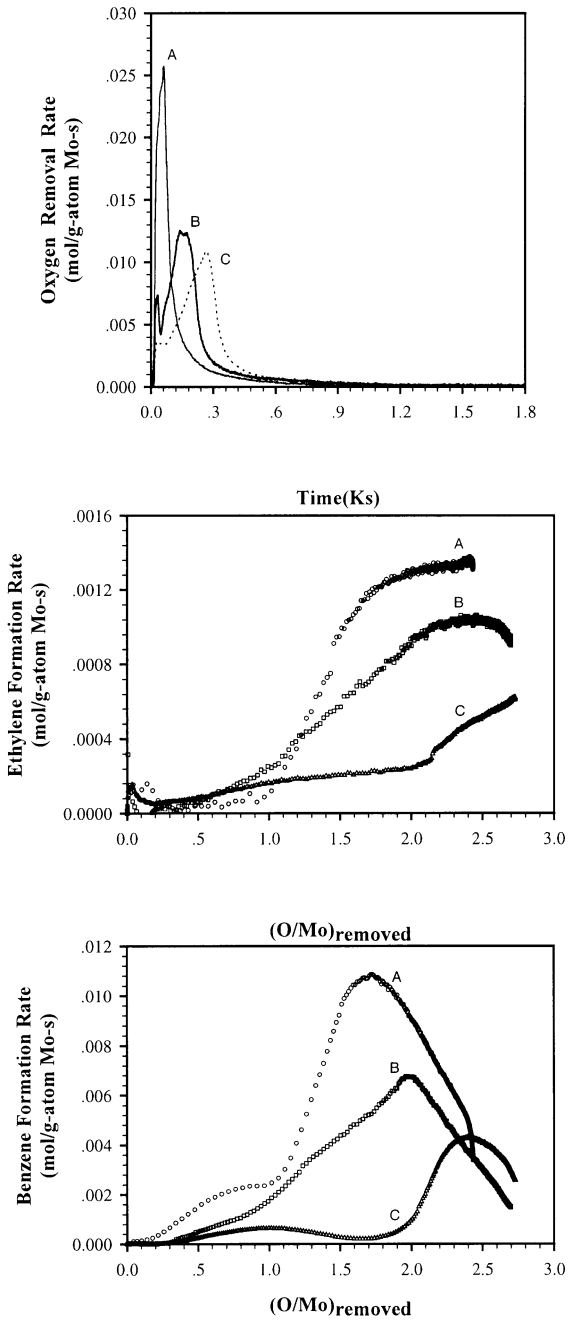

Fig. 12. Rates of total oxygen removed (top), C_2H_4 (middle) and benzene (bottom) formation rate as a function of cumulative oxygen removed $(O/Mo)_{removed}$ during initial reduction–carburization. (reaction conditions: as in Figs. 6 and 7). (A) 1.07% Mo, 0.5 g, space velocity 0.61 mol CH_4/g-atom Mo-s; (B) 3.60% Mo, 0.125 g, space velocity 0.65 mol CH_4/g-atom Mo-s; (C) 3.60% Mo, 0.5 g, space velocity 0.16 mol CH_4/g-atom Mo-s.

Increasing the space velocity also influences ethylene (Fig. 12) and benzene (Fig. 12) formation rates. The delay initially observed on the 3.6 wt% Mo/H–ZSM-5 samples is markedly shortened when the space velocity is increased from 0.16 to 0.65 s^{-1} and formation rates approach those measured on the 1.07 wt% Mo samples at similar space velocity (0.61 s^{-1}). The remaining differences between the two samples at similar space velocities reflect the diffusional restrictions discussed in the previous paragraph.

3.4. Stoichiometry and properties of active Mo species during CH_4 conversion

In this section, the carbon and hydrogen contents of MoC_x species and of strongly bound carbonaceous deposits on Brønsted sites within zeolite channels are reported from measurements of the amounts of carbon removed during treatments in H_2 and air after CH_4 reactions at 950 K for 2 h. The initial CH_4 reaction rates on deactivated MoO_x/H–ZSM-5 catalysts can be restored by a treatment in pure H_2 at reaction temperatures (950 K), without the recurrence of an activation period [14]. This method restores near-equilibrium methane conversions, without requiring the complex temperature cycling involved in O_2 regeneration procedures used to remove carbon deposits and restore MoO_x species [6]. Product selectivities at a given CH_4 conversion were identical on fresh and H_2-regenerated catalysts. After extensive deactivation ($\sim$700 h on stream), initial rates could not be restored by H_2 at 950 K, but treatment in a 20% O_2–Ar mixture as the temperature is raised from 300 to 950 K at 0.16 K s^{-1} removed all carbon deposits and restored both the initial CH_4 conversion rates and selectivities and the activation period. Thus, it appears that long-term deactivation arises from carbon deposits and not from irreversible structural changes in ZSM-5 or MoC_x sites. H_2 removes carbon species responsible for the initial deactivation, but oxidation reactions are required in order to remove more refractory forms of carbon that form slowly during CH_4 conversion.

The amount of carbon removed during H_2 treatment (predominantly as CH_4) is much smaller than that removed during subsequent treatment in 20%

Table 4
Carbon removed from carburized Mo/H–ZSM-5 during temperature-programmed treatments in H_2 (TPR) and 20% O_2–He (TPO) (0.5 g, 100 cm^3/min, 0.16 K s^{-1}; carburized for 2 h in 1:1 CH_4/Ar, TPR: 5% H_2–Ar, TPO: 20% O_2–He)

		Carbon removed (C/Mo ratio)[a]		
	(Mo wt%)	1.1	2.0	3.6
	Mo/Al	0.106	0.217	0.388
TPR	CH_4 produced	1.70	1.31	1.00
TPO	CO	17.0	6.34	2.81
	CO_2	25.3	10.7	5.36
	H_2O	5.35	2.58	1.42
	TPO Total	42.3	17.0	8.17
	Total	44.0	18.3	9.17

[a] C/Mo is the ratio of carbon atoms per Mo atom.

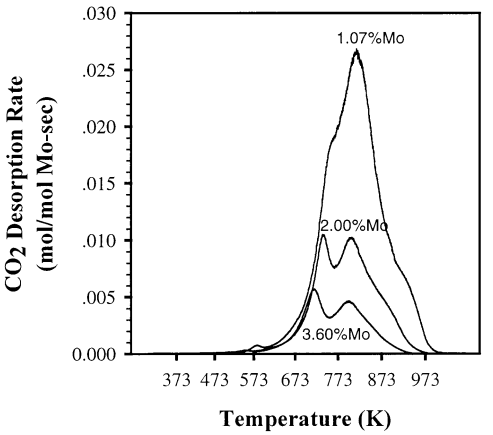

Fig. 13. TPO of MoC_x/H-ZSM-5 after carburization in CH_4–Ar at 950 K, 2 h (1–4 wt% Mo, 0.16 K s^{-1}, 100 cm^3/min 20% O_2–Ar) [after (1) 2 h carburization 100 cm^3/min 50% CH_4/Ar, 950 K; (2) 0.5 h reduction, 100 cm^3/min 20% H_2–Ar, 950 K; (3) 2 h carburization 100 cm^3/min 50% CH_4–Ar, 950 K; (4) TPR: 973 K, 0.16 K s^{-1}, 100 cm^3/min 5% H_2–Ar].

O_2–Ar. (Table 4). The latter removes all carbon species (Fig. 13) and restores fully initial CH_4 reaction rates, including the initial activation process. Two distinct desorption features were observed for all products (CO, CO_2, and H_2O). The area under the peak at ~723 K decreases with increasing Mo content, whereas that of the peak at higher temperatures (~823 K) increases as acid site concentration increases. The total amount of carbon desorbed was calculated from the sum of the CH_4 formed during H_2 treatment and the CO_x formed during oxidation (Table 4). MoC_x/H–ZSM-5 samples contain two types of sites: MoC_x species at exchange sites and residual acid sites (H^+). Both types of sites are likely to contain carbon and hydrogen during CH_4 reactions at 950 K.

If MoC_x and H^+ sites contain carbonaceous species, the carbon balance is given by

$$\frac{C}{Al} = M\left(\frac{H^+}{Al}\right) + N\left(\frac{Mo}{Al}\right), \quad (1)$$

where M carbon atoms reside at acid sites and N carbons at MoC_x sites. The number of acid sites remaining in these catalysts after treatment at 973 K can be estimated from D_2—OH and ^{27}Al NMR results (see Fig. 3). Dividing both sides of Eq. (1) by the Mo/Al ratio gives:

$$\frac{C}{Mo} = M\left(\frac{H^+}{Mo}\right) + N. \quad (2)$$

Fig. 14 shows the total C/Mo ratio obtained in

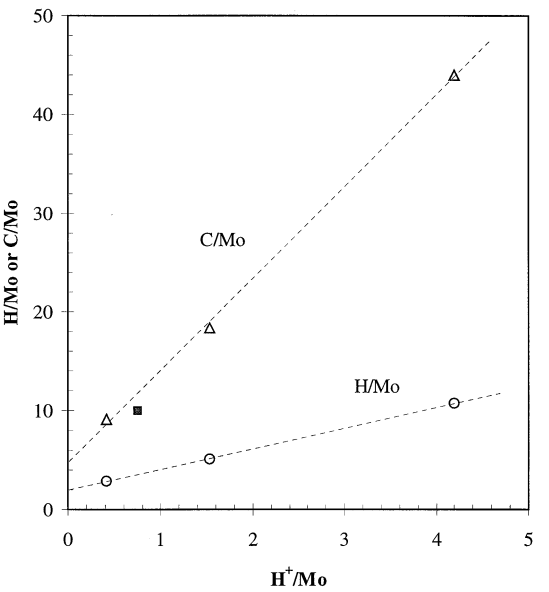

Fig. 14. C/Mo deposition during CH_4 aromatization at 950 K [1, 2, 4 wt% Mo/H–ZSM-5, CH_4/Ar (1:1), 100 cm^3/min, 1 h]. (N_2/CH_4 = 1:19, 2 wt% Mo/H–ZSM-5, Si/Al = 25, WHSV = 800 h^{-1} for 13 h, 973 K.) The solid square on the C/Mo line represents results calculated from Weckhuysen et al. [23].

the samples of this study as a function of the Brønsted acid site density from D_2—OH and ^{27}Al NMR results (see Fig. 3). The linear relation shown in Fig. 14 suggests that Brønsted acid sites contain about 9.3 carbon atoms per Brønsted acid site. The *y*-intercept corresponds to 4.8 carbon atoms per Mo. The Brønsted acid site density measurements in Fig. 14 have an uncertainty of about ± 0.05 [13], which translates to a range of 8.5–11.5 carbon atoms per H^+ and 4.0–6.8 carbon atoms per Mo. Weckhuysen et al. [23] reported the deposition of 10 carbon atoms per Mo on a 2 wt% Mo/H–ZSM-5 (Si/Al = 25) after CH_4 reaction at 973 K for 13 h, but the study did not address the relative amounts associated with acid and Mo sites. Their results (filled square in Fig. 14) are well within the range of those obtained in this study. A similar analysis of the amount of hydrogen removed as H_2O during treatment in O_2–Ar led to values of about two hydrogen atoms per acid site and also about two hydrogen atoms per Mo. These values, however, may not reflect the actual hydrogen content during CH_4 reactions, because the intervening H_2 treatment may have altered the hydrogen content of these carbonaceous deposits.

This analysis suggests that surface carbon species formed during CH_4 aromatization consist of species with nominal $C_{10}H_2$ stoichiometry on acid sites and with nominal C_5H_2 stoichiometry on Mo sites. The amount of carbon removed during TPR is proportional to the Mo concentration (Table 4), suggesting that the removal of only one or two C-atoms per Mo restores catalytic activity after H_2 regeneration by removing excess carbon from the MoC_x sites required for C—H bond activation in CH_4. Guisnet et al. [24] have detected the presence of multi-ring aromatic carbocations (C_{11}–C_{25}) on acid sites in H-ferrierite by dissolving the zeolite after *n*-butene isomerization reactions at 673 K and extracting aromatic species with methyl chloride. These results, our measured C/H^+ ratio of about 10, and the size constraints of ZSM-5 channels (0.55–0.57 nm), suggest that acid sites in Mo/H–ZSM-5 are covered during CH_4 reactions at 950 K with highly unsaturated aromatic carbocations with an average stoichiometry corresponding to dehydrogenated naphthalene or methyl-naphthalene species. These 'living carbocations' are alkylated by alkenes formed from methane and lead to the formation of observed products via β-scission reactions, as also proposed for methanol conversion to hydrocarbons on H–ZSM-5 [25–27].

Acknowledgements

Dr Young-Ho Kim was supported by the Korean Science and Engineering Foundation (KOSEF) during his sabbatical leave. Dr Richard Borry was supported by a National Science Foundation Fellowship. Project funding was provided by the Federal Energy Technology Center (US Department of Energy, contract DE-AC03-76SF00098) under the technical supervision of Dr Daniel Driscoll. ^{27}Al NMR experiments were performed in a collaboration with Ms Anne Huffsmith and Dr Jeffrey A. Reimer at the University of California at Berkeley, the results of which have been described in detail previously [13].

References

[1] T. Mole, J.R. Anderson, G. Creer, Appl. Catal. 17 (1985) 141.
[2] M.S. Scurrel, Appl. Catal. 32 (1987) 1.
[3] J.A. Biscardi, E. Iglesia, Catal. Today 31 (1996) 207.
[4] L. Wang, L. Tao, M. Xie, G. Xu, Catal. Lett. 21 (1993) 35.
[5] F. Solymosi, A. Erdohelyi, A. Szoke, Catal. Lett. 32 (1995) 43.
[6] D. Wang, J.H. Lunsford, M.P. Rosynek, Topics Catal. 3 (1996) 289.
[7] S. Liu, Q. Dong, R. Ohnishi, M. Ichikawa, J. Chem. Soc. Chem. Commun. (1997) 1455.
[8] A.Y. Stakheev, A.Y. Khodakov, L.M. Kustov, V.B. Kazansky, K.M. Minachev, Zeolites 12 (1992) 866.
[9] Y. Xu, Y. Shu, S. Liu, J. Huang, X. Guo, Catal. Lett. 35 (1995) 233.
[10] Y. Dong, S. Liu, Q. Zhang, J. Liu, K. Yang, Acta Petroleum Sinica (Petroleum Processing Section) 8 (1992) 66.
[11] Y. Xu, S. Liu, L. Wang, M. Xie, X. Guo, Catal. Lett. 135 (1995) 135.
[12] J.A. Biscardi, G.D. Meitzner, E. Iglesia, J. Catal. 179 (1998) 192.
[13] R.W. Borry, Y.-H. Kim, A. Huffsmith, J.A. Reimer, E. Iglesia, J. Phys. Chem. B103 (1999) 5787.
[14] F. Solymosi, A. Szoke, J. Cserenyi, Catal. Lett. 39 (1996) 157.

[15] W. Liu, Y. Xu, S.-T. Wong, L. Wang, J. Qiu, N. Yang, J. Mol. Catal. A: Chem. 120 (1997) 257.
[16] R.W. Borry, PhD Thesis, University of California at Berkeley, 1999.
[17] J.P. Wolthuizen, J.P. van den Berg, J.H.C. van Hoof, in: B. Imelik (Ed.), Catalysis by ZeolitesElsevier, Amsterdam, 1980..
[18] W. Li, R.W. Borry, G.D. Meitzner, E. Iglesia, J. Catal. (1999) submitted for publication.
[19] Y. Xu, W. Liu, S.-T. Wong, L. Wang, X. Guo, Catal. Lett. 40 (1996) 207.
[20] F. Solymosi, J. Cserenyi, A. Szoke, T. Bansagi, A. Oszko, J. Catal. 165 (1997) 150.
[21] S. Liu, L. Wang, R. Ohnishi, M. Ichikawa, J. Catal. 181 (1999) 175.
[22] H.S. Fogler, in: Elements of Chemical Reaction Engineering, third ed., Prentice Hall, 1998, p. 758.
[23] B.M. Weckhuysen, M.P. Rosynek, J.H. Lunsford, Catal. Lett. 52 (1998) 31.
[24] M. Guisnet, P. Andy, N.S. Gnep, C. Travers, E. Benazzi, in: H. Chou, S.-K. Ihm, Y.S. Uh (Eds.), Progress in Zeolite and Microporous Materials, Studies in Surface Science and Catalysis vol. 105, Elsevier, Amsterdam, 1997, p. 1365.
[25] I.M. Dahl, S. Kolboe, Catal. Lett. 20 (1993) 329.
[26] I.M. Dahl, S. Kolboe, J. Catal. 149 (1994) 458.
[27] E. Iglesia, T. Wang, S.Y. Yua, in: Studies in Surface Science and Catalysis vol. 119, Elsevier, Amsterdam, 1998, p. 527.